Catalysis Science & Technology

Accepted Manuscript

ROYAL SOCIETY OF CHEMISTRY

www.rsc.org/catalysis

Low temperature selective oxidation of methane to methanol using titania supported gold palladium copper catalysts.

Mohd Hasbi Ab Rahim[+], Robert D. Armstrong, Ceri Hammond, Nikolaos Dimitratos, Simon J. Freakley, Michael M. Forde, David J. Morgan, Georgi Lalev, Robert L. Jenkins, Jose Antonio Lopez- Sanchez, Stuart H. Taylor and Graham J. Hutchings*

Cardiff Catalysis Institute, School of Chemistry, Cardiff University Main Building, Park Place, Cardiff, CF10 3AT, United Kingdom. Tel: +44 (0) 2920874059, Fax: +44(0) 2090874 030

Current Address: [+] Faculty of Industrial Sciences & Technology, Universiti Malaysia Pahang, Lebuhraya Tun Razak, 26300, Kuantan, Pahang, Malaysia

*Corresponding author; Hutch@Cardiff.ac.uk

Abstract

The selective oxidation of methane to methanol has been studied using trimetallic AuPdCu/TiO_2 catalysts prepared by incipient wetness impregnation. They are able to catalyse the selective oxidation of methane to methanol under mild aqueous reaction conditions using H_2O_2 as the oxidant. When compared with bimetallic, Au-Pd/TiO_2 analogues, the new trimetallic catalysts present productivities which are up to 5 times greater under the same test conditions, and this is coupled with methanol selectivity of up to 83 %. Characterisation shows that whilst Au-Pd is present as Au- core Pd- shell nanoparticles, copper is present as either Cu or Cu_2O in < 5 nm particles.

Keywords

Methane, selective oxidation, methanol, AuPdCu, TiO_2, low temperature

1. Introduction

The direct oxidation of methane to methanol is a key challenge within the chemical sciences. Conventional natural gas reserves are estimated to exceed 200 trillion cubic meters [1], with further exploration ongoing. Owing to its high abundance, natural gas has been suggested as a fuel for society's transition away from a petroleum- dependent economy [2]. Direct conversion of the major components of natural gas (methane and ethane) to oxygenated products is a key challenge in achieving this. However, the direct catalytic upgrading of these short chain alkanes is yet to be achieved under mild/ green and industrially viable conditions. Processes for upgrading methane to value added products have been commercialised, however due to the relative inertness of the substrate ($\triangle H_{C\text{-}H}$ = 439.57 kJ mol^{-1}), these utilise harsh conditions for its activation [3]. Technologies for conversion of methane to methanol fall into two broad categories; indirect and direct. Indirect approaches utilise harsh conditions to convert methane to synthesis gas [4], which is then further converted to methanol, amongst other bulk chemicals. Although very selective, such processes have high energy and capital demands. Direct conversion of methane to methane- derivatives has also been reported. High temperature/ high pressure gas phase approaches have been reported [5], though these typically show low selectivity towards methanol. Methane oxidation in the liquid phase has also been

studied extensively. One approach involves oxidation of methane to yield methyl- esters [6-12] and often requires acidic media. The direct oxidation of methane to methanol is favourable, however, derivatization incurs additional workup and separation steps in the liquid phase. Several groups have used environmentally benign oxidants such as H_2O_2 in methane oxidation systems [13-26], though no system has as yet been deemed viable for commercialisation. Indeed, highly efficient H_2O_2 utilisation must be realised if H_2O_2 is to be used as the oxidant in the activation of methane. Circumventing the need to provide a premade H_2O_2 feed, liquid phase systems have been reported in which H_2O_2 is generated *in situ* from H_2 and O_2 [12]. However these systems used acid promoters and yielded formic acid or methyl esters as major products [11, 12].

It has previously been reported that supported AuPd catalysts catalyse the oxidation of methane with H_2O_2 at 50 ^oC in water [20, 21, 27]. The reaction was shown to proceed through formation of methylhydroperoxide which underwent further conversion to yield methanol and CO_2 [21]. The reaction was also performed in the absence of added H_2O_2, with H_2O_2 instead generated *in situ* from H_2 and O_2. In this way AuPd/TiO_2 catalysed both H_2O_2 synthesis and methane oxidation reactions [21]. We now extend these studies to show the effect of addition of copper to the previously reported catalyst systems. Catalysts are studied when H_2O_2 is both added and also generated *in situ*. We have assessed the effect of copper addition on the rate of H_2O_2 synthesis, methane activation, methanol selectivity and the efficiency with which H_2O_2 is utilised in products. Through catalyst characterisation studies, we aim to correlate catalyst structure and function.

2. Materials & Methods

2.1 Catalyst preparation

Supported catalysts were prepared by incipient wetness impregnation using chloride precursors. All loadings are given as wt%. The procedure for synthesis of a 2.5% Au 2.5% Pd 2.5% Cu/ TiO_2 catalyst is as follows;

Solutions of $HAuCl_4 \cdot 3H_2O$ (*Johnson Matthey*, 4.29 ml, 0.059 M) and $CuCl_2 \cdot 2H_2O$ (*Sigma* Aldrich, 5.3 ml, 0.149 M) were mixed, and then a solution of $PdCl_2$ (*Johnson Matthey*, 0.083 g) was added

with vigorous stirring. Following dissolution of the $PdCl_2$, TiO_2 (P25, *Degussa*, 1.85 g) was added with vigorous stirring. Once a homogeneous slurry was formed, drying was carried out (16 h, 110 ^oC). The dry catalyst was then ground to a fine powder and calcined in static air (400 ^oC, 3 h, 20 ^oC min^{-1}).

2.2 Catalyst Testing

2.2.1 Oxidation of methane with added *ex situ* H_2O_2

Catalyst testing was carried out in a 50 ml Teflon- lined stainless steel Parr autoclave reactor. The reactor was charged with H_2O_2 (*Sigma Aldrich*, 5000 μmol, 0.5 M) and catalyst (1.0 x 10^{-5} mol metal equivalent) was added. The reactor was sealed and purged 3 times with methane. The reactor was then charged with methane (*BOC*, 99.999 %, 30.5 bar) and the autoclave was heated to 50 ^oC. Once the setpoint temperature was reached, the system was vigorously stirred (1500 rpm) for 0.5 h. Following this the autoclave was cooled to *ca.* 12 ^oC to minimise loss of volatile products. Post reaction, the remaining H_2O_2 was quantified through titration versus acidified $Ce(SO_4)_2$ (8 x 10^{-3} mol dm^{-3}) of known concentration, with a Ferroin indicator. Aqueous products were quantified with solvent suppressed ^1H NMR at ambient temperature on a Bruker Ultrashield 500 MHz spectrometer using a TMS/ $CDCl_3$ internal standard. Gaseous products were quantified using a *Varian 450*-GC fitted with a CP-Sil 5CB capillary column (50 m length, 0.32 mm diameter, carrier gas = He), a methaniser unit and both FID and TCD detectors.

2.2.2 Oxidation of methane with *in situ* generated H_2O_2

Methane oxidation experiments with *in situ* generated H_2O_2 followed the same procedure as outlined in 2.2.1 with the following exceptions. Once sealed, the reactor was purged with 5% H_2/N_2 (*BOC*) and then charged with 5% H_2/N_2 (*BOC*), 25% O_2/N_2 (*BOC*) and CH_4 (*BOC*, 99.999%) such that the total pressure equalled 32 bar. The gas phase composition was 0.86% H_2/ 1.72% O_2/ 75.86 % CH_4/ 21.55% N_2 to ensure the mixture was outside of the explosive limits.

2.2.3 – H_2O_2 synthesis and decomposition

Hydrogen peroxide synthesis and hydrogenation was evaluated using a stainless steel Parr

autoclave with a nominal volume of 100 ml. The autoclave was charged with catalyst (0.01g) and 8.5 g solvent (5.6 g MeOH and 2.9 g H_2O). The charged autoclave was then purged three times with 5% H_2/CO_2 before pressurising with 5% H_2/CO_2 (29 bar) and 25% O_2/CO_2 (11 bar) at 20 ^oC. The temperature was then allowed to decrease to 2 ^oC followed by stirring (at 1200 rpm) of the reaction mixture for 30 mins. H_2O_2 productivity was determined by titrating aliquots of the final solution after reaction with acidified $Ce(SO_4)_2$ (0.01 M) in the presence of two drops of ferroin indicator.

H_2O_2 degradation experiments were carried out in a similar manner as H_2O_2 synthesis experiments but without adding the 25%O_2/CO_2. Furthermore, 0.68 g of H_2O from the 8.5 g of solvent was replaced by a 50 % H_2O_2 solution to give a reaction solvent containing 4 wt% H_2O_2. The standard reaction conditions for H_2O_2 hydrogenation included: 0.01 g catalyst, 8.5 g solvent (5.6 g MeOH, 2.22 g H_2O and 0.68 g H_2O_2 (50 %)), 29 bar 5%H_2/CO_2, 2 ^oC, 1200 rpm, 30 mins.

2.3 Catalyst Characterisation

Powder X-ray diffraction (XRD) patterns were collected on a PANalytical MPD diffractometer fitted with a $CuK_{\alpha 1}$ radiation source (λ= 0.154098 nm) at ambient conditions. Samples were scanned in the range of 10- 70 ^{o} at 40 kV and 40 mA.

HR-TEM was performed using a (LaB6) JEOL 2100 equipped with a high-resolution Gatan digital camera. In scanning transmission electron microscopy (STEM) mode, a dark field (HAADF/Z-contrast) detector was used. An EDS system (*Oxford Instruments*) equipped with a 80 mm^2 SDD (Silicon Drift Detector) X-Max^N 80 T was employed to study the elemental composition in Point & ID, Line scans, layered and elemental mapping modes. EDS data was analysed using AZtecTEM software. For HR-TEM analysis, samples were suspended in DI water and *ca*.1 μL was added to a TEM grid and dried. EDS analysis of the samples containing Cu was carried out using Ni TEM grids and a Beryllium sample holder.

X-Ray photoelectron spectroscopy (XPS) was performed using a VG EscaLab 220i spectrometer, using a standard Al-Kα X-ray source (300 W) and analyzer pass energy of 20 eV. Samples were mounted using double-sided adhesive tape, and binding energies were referenced to the C 1s binding energy of adventitious carbon contamination at 284.7 eV.

Temperature programmed reduction (TPR) profiles were obtained using a ThermoElectron TPDRO 1100 instrument fitted with a TCD. Catalysts were pretreated at 90 ^{o}C under a flow of He (20 mL min^{-1}) for 0.5 h and then allowed to cool to ambient temperature. The flow was then switched to 10 % H_2/Ar (15 mL min^{-1}) and the temperature was raised to 700 ^{o}C using a linear ramp rate of 5 ^{o}C min^{-1}.

3. Results and Discussion

3.1 Liquid Phase oxidation of methane with preformed H_2O_2

Our previous studies have shown TiO_2 to be an effective support for methane activation over bimetallic AuPd catalysts [21]. Whilst inactive in the reaction, the addition of TiO_2 to a homogeneous $HAuCl_4 \cdot H_2O$ catalysed methane oxidation reaction resulted in an increase of methanol selectivity and decreased selectivity towards formic acid [20]. In a similar way, studies into the oxidation of methane over ZSM-5 catalysts have reported that deposition of Cu^{2+} increases methanol selectivity dramatically by preventing further oxidation to formic acid. EPR studies showed that Cu^{2+} was either scavenging or preventing formation of hydroxyl radicals [24, 25]. Indeed, theoretical studies have reported Cu to be capable of oxidising methane to methanol [28]. As copper has both been reported to increase selectivity to primary products and is able to oxidise methane to methanol we investigated the possibility of adding Cu as a component to supported AuPd catalysts.

A series of mono, bi and tri- metallic catalysts comprising Au/Pd/Cu were prepared and tested for oxidation of methane with H_2O_2 added as the oxidant (Table 1). For comparison with previously published data, Table 1 Entry 1 presents previously published data for the optimal catalyst (2.5 % Au 2.5% Pd/ TiO_2 prepared by the incipient wetness impregnation method) [21].

When deposited onto TiO_2 at 2.5 wt% loading, Cu is itself active (Table 1 Entry 2) which is consistent with the ability of Cu to catalyse Fenton's type H_2O_2 conversion and generate oxygen based radical

species [29, 30]. Indeed, the methane oxidation products methylhydroperoxide, methanol and CO_2 were observed in the reaction mixture. The overall activity of this catalyst was higher than that of the previously reported bimetallic AuPd catalyst (Table 1 Entry 1) with a TOF of 1.0 compared to 0.70 mol $_{methane\ converted}$ mol $_{metal}^{-1}$ h^{-1}, and H_2O_2 was more efficiently utilised with 4.9 % of active oxygen retained in the products. This is compared with 2.1 % for AuPd/TiO_2. Moreover, monometallic Cu/TiO_2 displayed higher selectivity towards partially oxygenated products at 96 %, which is compared with 90 % for the 2.5% Au 2.5% Pd catalyst. The opposite trend was observed in methanol selectivity however, with 49% for the AuPd catalyst and 14% for monometallic Cu. This suggests that Cu does not catalyse the transformation of methylhydroperoxide to methanol at rates which are comparable to AuPd catalysts. Co-deposition of 2.5 wt% Cu and 2.5 wt% Au increased oxygenate productivity with no change in the product distribution. An added benefit of Au addition was an increase in efficiency of H_2O_2 usage to 6.7 %. Both Au- Cu and Pd- Cu catalysts showed lower methanol selectivity than the Au-Pd catalyst, with methylhydroperoxide the favoured reaction product (83 % and 66 % respectively).

Clearly both Au and Pd are required to effectively convert methylhydroperoxide to methanol. Hence, combining the high catalytic activity afforded by Cu and high methanol selectivity of AuPd nanoparticles would be desirable in a trimetallic catalyst. Addition of 2.5 wt% Cu to a 2.5% Au 2.5% Pd catalyst led to a fivefold increase in catalyst productivity compared with the bimetallic AuPd (Table 1 Entry 1). This constituted a 135 % increase in TOF from 0.7 to 1.65 mol $_{methane\ converted}$ mol $_{metal}^{-1}$ h^{-1}. Once more, addition of Cu led to increased efficiency of H_2O_2 utilisation, reaching 12.2% whilst H_2O_2 conversion decreased from 93 % to just 50 %. This suggests that Cu is either altering the AuPd active sites by (i) changing the redox properties of active sites (ii) blocking active sites of non-desirable H_2O_2 decomposition pathways, or (iii) that Cu is itself altering the rate of H_2O_2 decomposition. This is explored later in this paper. As with Au- Cu and Pd- Cu catalysts, addition of Cu shifted the product distribution to favour the primary product methylhydroperoxide (69 % selectivity). Indeed, methanol selectivity for the AuPdCu catalyst (7.5 wt% metal loading, Table 1 Entry 5) was 27.8 % which is compared with 49.3 % for the Au-Pd catalyst (Table 1 Entry 1). This

effect of Cu is consistent with previous Cu/ZSM-5 studies, whereby Cu^{2+} was shown to inhibit the hydroxyl radical- mediated oxidation of methanol to formic acid [24, 25]. The wt% loading of Cu was therefore decreased, to determine whether higher methanol selectivity might be achieved whilst still minimising the unselective decomposition of H_2O_2. Comparable activity to 2.5% Au 2.5% Pd 2.5% Cu/TiO_2 was observed upon testing of a 2.5% Au 2.5% Pd 1% Cu/TiO_2 catalyst, with TOF (h^{-1}) of 1.65 and 1.40 respectively. Through lowering of the Cu loading, methanol selectivity increased from 27.8 % to 82.7 %, with H_2O_2 conversion also increasing to 83 %. Catalyst performance for this trimetallic catalyst is superior to that of our previously reported AuPd catalyst (Table 1 Entry 1) under liquid phase conditions [21]. Furthermore, addition of Cu led to decreased CO_2 selectivity from 9.7% for $Au\text{-}Pd/TiO_2$ to 3.1 and 4.5% following deposition of 2.5 wt% and 1.0 wt% Cu respectively. Finally, a physical mixture of 2.5% Au 2.5% Pd/ TiO_2 and 2.5% Cu/TiO_2 was tested and showed a comparatively low TOF of 0.34 and high rate of H_2O_2 decomposition relative to its trimetallic analogue. This suggested a synergistic interaction when Au/Pd and Cu are in close proximity.

3.2 Liquid phase oxidation of methane with *in situ* generated H_2O_2

Addition of Cu to AuPd catalysts has been shown to enhance catalytic activity and selectivity for the oxidation of methane to methanol with added H_2O_2 as oxidant. A series of trimetallic AuPdCu/ TiO_2 catalysts of varying wt % Cu loading was therefore prepared and assessed for catalytic activity in the oxidation of methane with H_2O_2 generated *in situ* from H_2 and O_2. Catalytic data for the optimal bimetallic AuPd catalyst from our previous studies is shown in Table 2 Entry 1.

Co- deposition of Cu with AuPd (Table 2 Entries 2-5) led to a significant decrease in catalytic activity for methane oxidation when H_2O_2 was produced *in situ*. Deposition of Cu onto AuPd might alter or block the active sites responsible for generating H_2O_2 from dissolved H_2 and O_2 and thereby limit oxidant availability for the methane oxidation reaction. To explore this, catalysts were tested for activity in the synthesis and degradation of H_2O_2 under previously reported reaction conditions [31]. It is apparent (Table 3) that addition of Cu to 2.5% Au 2.5% Pd/ TiO_2 has a detrimental effect upon the net rate of H_2O_2 synthesis, with catalyst productivity falling from 83 mol kg^{-1} h^{-1} to 10 and 11 for Cu loadings of 1.0 wt% and 2.5 wt% respectively. The rate of H_2O_2 degradation is also lower for the

trimetallic catalysts (Table 3, Entries 2 and 3). This represents combined rates of H_2O_2 hydrogenation and decomposition pathways. Given that addition of Cu also led to decreased H_2O_2 synthesis rates, it can therefore be concluded that Cu blocks the sites needed for H_2 activation to H_2O_2. This indicates that the decomposition pathway would dominate the degradation rates in Table 3 Entries 2 and 3. The ability of Cu to decompose H_2O_2 at 50 ^oC was studied under an inert atmosphere of N_2 (P = 30 bar) with all other test conditions set as in Table 1 (0.5 h, $[H_2O_2]$ = 0.5 M, 5000 μmol, 50 ^oC, 1500 rpm, 1.0 x 10^{-5} mol of metal – 25.4 mg catalyst). Upon testing, 2.5% Cu/TiO_2 showed a high H_2O_2 decomposition rate of 384 mol $_{H2O2\ converted}$ kg_{cat}^{-1} h^{-1}. This is compared with a rate of 0.406 mol $_{methane\ converted}$ kg_{cat}^{-1} h^{-1} when the same catalyst was tested for methane oxidation at 50 ^oC with added H_2O_2 (0.5 M, 5000 μmol, Table 1 Entry 2). The low oxygenate productivities shown for trimetallic catalysts in Table 2 can therefore be attributed to competition between a high rate of Cu- catalysed H_2O_2 decomposition and low rates of H_2O_2 synthesis/ methane oxidation reactions. This was confirmed through addition of 2.5 % Cu/TiO_2 to a reaction catalysed by 2.5% Au 2.5% Pd/TiO_2. Physical mixing of these catalysts led oxygenate productivity to fall from 0.11 mol $_{methane\ converted}$ kg_{cat}^{-1} h^{-1} to 0.074 mol $_{methane\ converted}$ kg_{cat}^{-1} h^{-1} (Table 2, Entry 7). This is comparable to the productivity of 0.068 (same units) which was observed for 2.5% Au 2.5% Pd 2.5% Cu/TiO_2 under the same reaction conditions (Table 2, Entry 2).

3.3 Catalyst characterisation

To correlate catalyst performance and structural/ electronic properties, catalysts were characterised using XRD, TEM, XPS and H_2-TPR.

X-ray diffraction patterns of the mono, bi and tri- metallic Au/Pd/Cu catalysts from studies in Table 1 were recorded and are shown in Figure 1. Comparison with reference patterns for Cu^0 (JCPDS no: 01-085-1326), CuO (JCPDS no: 01-089-5986) (CuO) and Cu_2O (JCPDS no: 01-071-3645) showed no peaks corresponding to copper species for mono bi or tri- metallic Cu- containing catalysts. This suggests that the crystallite size of supported copper species is below the detection limit of the instrument. Characteristic signals for metallic Au were observed at 2θ = 38.2 ^{o}, 44.3 ^{o} and 64.5 ^{o} in Au-containing samples. These are assigned to the (111), (200) and (311) planes respectively (JCPDS no.

03-065-2870). No Pd phases were observed in the monometallic Pd catalyst (Figure 1 d). In all samples the characteristic peaks of the TiO_2 (P25) support were clearly observed (Figure 1 a). Based upon the diffraction peak at 44.3°, the mean Au crystallite size for 2.5% Au 2.5% Pd 2.5% Cu/TiO_2 was calculated to be 18.5 nm, using the Scherrer equation. This increased to 23.5 nm for 2.5% Au 2.5% Pd 1.0% Cu/TiO_2. Au- catalysts contained Au in a cubic phase with comparable unit cell parameters to monometallic Au (ICSD no. 53764) as shown in Table 4. No apparent alloying of Au/Pd and Cu was observed in XRD diffractograms. Although no reflections indicative of bulk alloyed nanoparticles were observed, a portion of nanoparticles which are beneath the detection limit of the XRD method could be present. To determine whether this was indeed the case, catalysts were studied using HRTEM. Micrographs and corresponding particle size distributions are shown in Figure 2. Based upon a sample of 530 nanoparticles the catalysts; 2.5% Au 2.5% Pd/TiO_2, 2.5% Au 2.5% Pd 1.0 % Cu/TiO_2 and 2.5% Au 2.5% Pd 2.5% Cu /TiO_2 showed average nanoparticle sizes of 1.32, 1.20 and 1.37 nm respectively. Due to restrictive particle dimensions, visualisation of core shell features was not possible. However, previous studies of AuPd/ TiO_2 catalysts prepared via the same impregnation method described in Section 2.1 have shown Au- core Pd- rich shell nanoparticles to form upon calcination at 400 °C in air [32]. We rationalised the disparity between average particle sizes as determined by XRD (Scherrer, Figure 1) and HRTEM (Figure 2) methods using STEM-EDX. This showed the presence of ~ μm sized gold- rich particles (Supporting Information Figure S1). Formation of large (200 nm – 2 μm) Au- rich particles, and Au- core/ Pd-rich shell nanoparticles during impregnation of TiO_2 with $HAuCl_4.6H_2O$ and $PdCl_2$ is consistent with previous work by Meenakshisundaram *et al* [33].

XPS spectra were collected to evaluate the oxidation state and surface composition of Cu, Pd and Au species present in 2.5% Au 2.5% Pd 1% Cu/TiO_2 following calcination (Figure 3). Copper species of differing oxidation state show characteristic binding energies and satellite structures with Cu^{2+} (934 eV) species exhibiting a shakeup peak at *ca.* 10 eV above the Cu ($2p_{3/2}$) signal [34, 35]. These peaks are not observed for Cu^{+} or Cu^{0} and can therefore be used to differentiate between $Cu^{2+}$and reduced species [34, 36]. The Cu (2p) spectra for 2.5% Au 2.5% Pd 2.5% Cu/TiO_2, both before and after

calcination, are shown in Figure 3 (a) and (b) respectively. The main peak is observed at a binding energy of 932.8 eV and attributed to reduced Cu species (Cu^{I} / Cu^{+}) suggesting either Cu_2O or metallic Cu. A minor Cu^{2+} contribution is also observed as a weak shoulder at 934 eV and a weak satellite peak at 944 eV.

The corresponding Au (4d)/Pd (3d) spectra for the same catalysts are shown in Figure 4 (a) and (b). It is evident that prior to calcination the spectrum is composed of Pd (3d) peaks superimposed on the Au ($4d_{5/2}$) peak (ca 335 eV). Pd is present as Pd^{2+}, as evidenced by the binding energy of 337.6 eV, whilst the presence of any Pd (0) in this uncalcined sample could not be ascertained due to a strong overlap with the Au signal.

Following calcination Pd is present as both Pd^{2+} (337.8 eV) and Pd (0) (335.3 eV) in an atomic ratio of 6.14: 1 (Figure 3 b). After heat treatment no signal corresponding to Au (4d) is observed (Figure 3 b) whereas a significant attenuation of the Au (4f) signal at 83.8 eV is apparent (Figure 3 c and d). The Au(4f) signal is observable over the Au(4d) signal due to the difference in the mean free path of the photoelectron at the different kinetic energies.

A summary of quantified surface- metal composition of the uncalcined and calcined catalysts is given in Table 5. Following heat treatment a significant decrease in Au surface concentration is observed, with the Pd/Au atomic ratio increasing from 0.54 to 15.17. A similar increase in the Cu/Au ratio also occurred. This indicates that Au core – Pd shell alloyed nanoparticles are formed upon calcination, and the increase in Pd/Au ratio is consistent with aforementioned attenuation of the Au signal, which is analogous to the observed attenuation by Pd overlayers as previously reported by Edwards *et al.* for AuPd/ TiO_2 catalysts prepared under comparable conditions [32]. Furthermore, quantitative analysis in Table 5 suggests that following heat treatment the TiO_2 surface is enriched with both Pd and Cu. Cu enrichment could arise from; formation of Au- core PdCu- shell nanoparticles or Cu being more highly dispersed across the TiO_2 surface than Au. XRD data shown in Figure 1 and the low Cu loadings used support the latter. Little change in the Pd/Cu ratio is apparent in Table 5, indicating that core shell Pd- Cu species are not forming. XPS surface analysis of 2.5% Pd 2.5% Cu/TiO_2 (Table 5 Entry 3) shows a Pd: Cu ratio of *ca*. 1, which further supports this. Therefore, whereas Pd-Cu alloying

has been reported for supported TiO_2 catalysts following heat treatment in hydrogen [37], calcination in static air appears to favour surface segregation between Pd and Cu. Future EDX mapping studies at a higher resolution are required to determine whether Pd and Cu are indeed phase- segregated.

H_2-TPR was carried out on Au/Pd/Cu/ TiO_2 catalysts to probe the reducibility of metal sites and determine the nature of supported metal species. No reduction was observed in the TPR of unmodified TiO_2 (P25) shown in Figure 5 a. Deposition of 2.5% Cu (Figure 5 b) gave rise to a single major reduction peak centred at 180 ^oC. This was assigned to a 2 electron Cu^{II} _ Cu^0 reduction in highly dispersed CuO species [38]. The monometallic Cu catalyst also presented a second, less intense reduction centred at 300 ^oC, which was assigned to reduction of larger particles of bulk CuO on the surface of TiO_2 [39]. TPR data suggested that no Au-Cu alloys are present in bi and trimetallic catalysts (Figure 5 b and c). If Au- Cu alloys were formed in bimetallic (c) or trimetallic (d) catalysts, an additional reduction peak would be expected at *ca*. 260 – 280 ^oC [38, 40]. Given that the catalysts in this study were calcined in air (3 h at 400 ^oC), alloy formation would not be expected. Indeed, Bracey *et al.* have previously reported minimal interaction between Au and Cu under such heat treatment conditions [41]. Disappearance of the Cu^{II}- Cu^0 reduction event at 180 ^oC in the trimetallic catalyst (c) is in agreement with XPS data from Figure 3, which suggests that Cu presents as reduced species following calcination. Figure 5 (e) shows the reduction profile for 2.5% Au 2.5% Pd/TiO_2. This catalyst is known to contain alloyed AuPd nanoparticles [21]. Comparison with the reduction profile of 2.5% Au 2.5% Pd 1.0% Cu/TiO_2 (Figure 5 d) suggests that the trimetallic catalyst also contains alloyed AuPd nanoparticles. Meanwhile, the negative peak observed at *ca*. 95 ^oC in Figures 4 (d) and (e) is assigned to the low temperature decomposition of palladium hydride species [42, 43].

Catalyst characterisation showed that in trimetallic AuPdCu/ TiO_2 catalysts, Au- core Pd- shell nanoparticles form upon calcination at 400^oC in static air. This was found to be consistent with previous studies [21, 32]. Though no alloying of Au/Pd and Cu is observed, copper speciation was effected by the presence of Pd, with Cu^{II} favoured in Cu / AuCu catalysts and Cu^0 / Cu^I species in trimetallic AuPdCu catalysts. Trimetallic catalysts showed increased productivity and TOF for the oxidation of methane with added H_2O_2 when compared with either bimetallic AuPd catalysts or a

physical mixture of AuPd/$TiO_2$and Cu/TiO_2. As Cu^I can catalyse the conversion of H_2O_2 to oxygen based radicals in a Cu^I/Cu^{II} redox couple, an increase in rate is expected. However the decrease in the rate of H_2O_2 conversion and simultaneous increase in rate of methane oxidation observed following impregnation of Cu onto 2.5% Au 2.5% Pd/TiO_2 (Table 1 Entries 5 and 6) suggest an additional role of Cu in blocking Au/Pd sites, which would otherwise catalyse H_2O_2 decomposition in a non-selective way. Future studies should therefore further characterise these trimetallic catalysts to probe for Cu – Au/Pd interactions and map the atomic composition/ distribution of constituent nanoparticles.

4. Conclusions

Trimetallic AuPdCu catalysts are active for the oxidation of methane under mild reaction conditions using the green oxidant H_2O_2. We have shown that by depositing copper together with Au/Pd on the surface of TiO_2 the rate of methane oxidation with added H_2O_2 is significantly enhanced. In particular 2.5% Au 2.5% Pd 1.0% Cu/TiO_2 showed *ca*. 83% selectivity to methanol, a significant improvement on the 49.3% selectivity previously reported for a bimetallic 2.5% Au 2.5% Pd/ TiO_2 analogue. At the same time deposition of 2.5 wt% Cu increased catalyst productivity by a factor of 5. Furthermore, through control of the Cu/ AuPd ratio catalysts might be tailored to effect either high methanol selectivity or increased efficiency in H_2O_2 utilisation. These catalysts were tested for the oxidation of methane with H_2O_2 generated *in situ* from H_2 and O_2. In this instance the addition of Cu was disadvantageous, leading to a decrease in the rate of methane oxidation. This trend was attributed to low rates of H_2O_2 synthesis coupled with competing Cu- catalysed H_2O_2 conversion reactions, which proceed at far higher rates than the oxidation reaction. Characterisation studies of these trimetallic catalysts using XRD, XPS and H_2-TPR indicate that Au and Pd alloy in an Au- core Pd- shell structure, whilst Cu is highly dispersed as reduced species, probably as Cu_2O or Cu. The beneficial effect of Cu is ascribed to its ability to direct the selective catalytic conversion of H_2O_2. The mechanism by which specific Cu sites effect selective conversion of H_2O_2, and its impact upon reaction rates in partial alkane oxidation will be explored in a future paper.

Acknowledgements

This work formed part of the Dow Methane Challenge. The DOW Chemical Company is thanked for their financial support.

References

1. F. Holz, P. M. Richter and R. Egging, *Review of Environmental Economics and Policy*, 2015, DOI: 10.1093/reep/reu016.
2. G. A. Olah, *Angewandte Chemie International Edition*, 2005, 44, 2636-2639.
3. S. J. Blanksby and G. B. Ellison, *Accounts Chem. Res.*, 2003, 36, 255-263.
4. M. A. Pena, J. P. Gomez and J. L. G. Fierro, *Appl. Catal., A*, 1996, 144, 7-57.
5. N. R. Hunter, H. D. Gesser, L. A. Morton, P. S. Yarlagadda and D. P. C. Fung, *Appl. Catal.*, 1990, 57, 45-54.
6. WO2014130987A1, 2014.
7. R. A. Periana, D. J. Taube, E. R. Evitt, D. G. Löffler, P. R. Wentrcek, G. Voss and T. Masuda, *Science*, 1993, 259, 340-343.
8. R. A. Periana, D. J. Taube, S. Gamble, H. Taube, T. Satoh and H. Fujii, *Science*, 1998, 280, 560-564.
9. N. Basickes, T. E. Hogan and A. Sen, *Journal of the American Chemical Society*, 1996, 118, 13111-13112.
10. M. M. Konnick, B. G. Hashiguchi, D. Devarajan, N. C. Boaz, T. B. Gunnoe, J. T. Groves, N. Gunsalus, D. H. Ess and R. A. Periana, *Angew. Chem., Int. Ed.*, 2014, 53, 10490-10494.
11. E. D. Park, Y. S. Hwang and J. S. Lee, *Catalysis Communications*, 2001, 2, 187-190.
12. E. D. Park, Y.-S. Hwang, C. W. Lee and J. S. Lee, *Applied Catalysis A: General*, 2003, 247, 269-281.
13. M. M. Forde, B. C. Grazia, R. Armstrong, R. L. Jenkins, M. H. A. Rahim, A. F. Carley, N. Dimitratos, J. A. Lopez-Sanchez, S. H. Taylor, N. B. McKeown and G. J. Hutchings, *Journal of Catalysis*, 2012, 290, 177-185.
14. T. Osako, E. J. Watson, A. Dehestani, B. C. Bales and J. M. Mayer, *Angewandte Chemie International Edition*, 2006, 45, 7433-7436.
15. A. K. M. L. Rahman, R. Indo, H. Hagiwara and T. Ishihara, *Applied Catalysis A: General*, 2013, 456, 82-87.
16. A. K. M. L. Rahman, M. Kumashiro and T. Ishihara, *Catalysis Communications*, 2011, 12, 1198-1200.
17. G. B. Shul'pin, T. Sooknoi, V. B. Romakh, G. Süss-Fink and L. S. Shul'pina, *Tetrahedron Letters*, 2006, 47, 3071-3075.
18. G. B. Shul'pin, G. V. Nizova, Y. N. Kozlov, L. Gonzalez Cuervo and G. Süss-Fink, *Advanced Synthesis & Catalysis*, 2004, 346, 317-332.
19. A. B. Sorokin, E. V. Kudrik and D. Bouchu, *Chemical Communications*, 2008, 2562-2564.
20. M. Ab Rahim, M. Forde, C. Hammond, R. Jenkins, N. Dimitratos, J. Lopez-Sanchez, A. Carley, S. Taylor, D. Willock and G. Hutchings, *Top Catal*, 2013, 56, 1843-1857.
21. M. H. Ab Rahim, M. M. Forde, R. L. Jenkins, C. Hammond, Q. He, N. Dimitratos, J. A. Lopez-Sanchez, A. F. Carley, S. H. Taylor, D. J. Willock, D. M. Murphy, C. J. Kiely and G. J. Hutchings, *Angewandte Chemie*, 2013, 125, 1318-1322.
22. M. M. Forde, R. D. Armstrong, R. McVicker, P. P. Wells, N. Dimitratos, Q. He, L. Lu, R. L. Jenkins, C. Hammond, J. A. Lopez-Sanchez, C. J. Kiely and G. J. Hutchings, *Chemical Science*, 2014, 5, 3603-3616.
23. C. Hammond, N. Dimitratos, R. L. Jenkins, J. A. Lopez-Sanchez, S. A. Kondrat, M. Hasbi ab Rahim, M. M. Forde, A. Thetford, S. H. Taylor, H. Hagen, E. E. Stangland, J. H. Kang, J. M. Moulijn, D. J. Willock and G. J. Hutchings, *ACS Catalysis*, 2013, 3, 689-699.

24. C. Hammond, M. M. Forde, M. H. Ab Rahim, A. Thetford, Q. He, R. L. Jenkins, N. Dimitratos, J. A. Lopez-Sanchez, N. F. Dummer, D. M. Murphy, A. F. Carley, S. H. Taylor, D. J. Willock, E. E. Stangland, J. Kang, H. Hagen, C. J. Kiely and G. J. Hutchings, *Angewandte Chemie International Edition*, 2012, 51, 5129-5133.
25. C. Hammond, R. L. Jenkins, N. Dimitratos, J. A. Lopez-Sanchez, M. H. ab Rahim, M. M. Forde, A. Thetford, D. M. Murphy, H. Hagen, E. E. Stangland, J. M. Moulijn, S. H. Taylor, D. J. Willock and G. J. Hutchings, *Chemistry – A European Journal*, 2012, 18, 15735-15745.
26. N. Mizuno, Y. Seki, Y. Nishiyama, I. Kiyoto and M. Misono, *J. Catal.*, 1999, 184, 550-552.
27. WO2011051642A1, 2011.
28. Y. Shiota and K. Yoshizawa, *J. Am. Chem. Soc.*, 2000, 122, 12317-12326.
29. T. Ozawa and A. Hanaki, *J. Chem. Soc., Chem. Commun.*, 1991, DOI: 10.1039/c39910000330, 330-332.
30. A. N. Pham, G. Xing, C. J. Miller and T. D. Waite, *Journal of Catalysis*, 2013, 301, 54-64.
31. J. C. Pritchard, Q. He, E. N. Ntainjua, M. Piccinini, J. K. Edwards, A. A. Herzing, A. F. Carley, J. A. Moulijn, C. J. Kiely and G. J. Hutchings, *Green Chemistry*, 2010, 12, 915-921.
32. J. K. Edwards, B. E. Solsona, P. Landon, A. F. Carley, A. Herzing, C. J. Kiely and G. J. Hutchings, *J. Catal.*, 2005, 236, 69-79.
33. M. Sankar, Q. He, M. Morad, J. Pritchard, S. J. Freakley, J. K. Edwards, S. H. Taylor, D. J. Morgan, A. F. Carley, D. W. Knight, C. J. Kiely and G. J. Hutchings, *ACS Nano*, 2012, 6, 6600-6613.
34. J. Batista, A. Pintar, D. Mandrino, M. Jenko and V. Martin, *Appl. Catal., A*, 2001, 206, 113-124.
35. K. S. Kim, *J. Electron Spectrosc. Relat. Phenomena*, 1974, 3, 217-226.
36. J. A. Rodriguez, J. Y. Kim, J. C. Hanson, M. Perez and A. I. Frenkel, *Catal. Lett.*, 2003, 85, 247-254.
37. F. Zhang, S. Miao, Y. Yang, X. Zhang, J. Chen and N. Guan, *J. Phys. Chem. C*, 2008, 112, 7665-7671.
38. R. J. Chimentao, F. Medina, J. L. G. Fierro, J. Llorca, J. E. Sueiras, Y. Cesteros and P. Salagre, *J. Mol. Catal. A: Chem.*, 2007, 274, 159-168.
39. C.-S. Chen, J.-H. You, J.-H. Lin and Y.-Y. Chen, *Catal. Commun.*, 2008, 9, 2381-2385.
40. J. Llorca, M. Dominguez, C. Ledesma, R. J. Chimentao, F. Medina, J. Sueiras, I. Angurell, M. Seco and O. Rossell, *J. Catal.*, 2008, 258, 187-198.
41. C. L. Bracey, A. F. Carley, J. K. Edwards, P. R. Ellis and G. J. Hutchings, *Catal. Sci. Technol.*, 2011, 1, 76-85.
42. A. M. Eberhardt, E. V. Benvenutti, C. C. Moro, G. M. Tonetto and D. E. Damiani, *J. Mol. Catal. A: Chem.*, 2003, 201, 247-261.
43. U. S. Ozkan, M. W. Kumthekar and G. Karakas, *Catal. Today*, 1998, 40, 3-14.

Table 1 Methane oxidation activity of mono, bi or trimetallic Cu/Au/Pd/ TiO_2 catalysts

Entry	Catalyst	Product amount / μmol				Oxygenate Selectivity / % [a]	Methanol Selectivity / %	Oxygenate Productivity [b]	TOF [c]	H_2O_2 Remain / μmol [d]	H_2O_2 efficiency [e]
		CH_3OH	HCOOH	CH_3OOH	CO_2						
1	2.5 % Au 2.5 % Pd/ TiO_2	1.89	0	1.57	0.37	90	49.3	0.250	0.70	383	2.1
2	2.5 % Cu/TiO_2	0.76	0	4.40	0.19	96	14.2	0.406	1.03	338	4.9
3	2.5 % Au 2.5 % Cu/ TiO_2	0.91	0	6.18	0.39	95	12.2	0.739	1.42	66	6.7
4	2.5 % Pd 2.5 % Cu/ TiO_2	0.64	0	2.30	0.56	84	18.3	0.369	0.59	2434	5.6
5	2.5 % Au 2.5 % Pd/ 2.5 % Cu/TiO_2	2.36	0	5.87	0.26	97	27.8	1.243	1.65	2483	12.2
6	2.5 % Au 2.5 % Pd/ 1.0 % Cu/TiO_2	6.08	0	0.94	0.33	96	82.7	0.729	1.40	842	1.5
7	2.5 % Au 2.5 % Pd /TiO_2 and 2.5 % Cu/TiO_2*	0.49	0	1.23	0.34	83	23.8	0.128	0.34	845	1.9

Test conditions: 0.5 h, 50 ^oC, P(CH_4) = 30 bar, Catalyst: 1.0 x 10^{-5} mol of metal., [H_2O_2] = 0.5 M (5000 μmol), 1500 rpm

[a]Oxygenate selectivity = (mol of oxygenate/ total mol of products) * 100, [b] Oxygenates productivity = mol $_{oxygenates}$ kg_{cat}^{-1} h^{-1}, [c] Turn over frequency (TOF) = mol $_{oxygenates}$ mol $_{metal}^{-1}$ h^{-1}, [d] Assayed by Ce^{+4} (aq) titration. [e] (mol O_2 in products/ mol H_2O_2 converted) *100 [f] Pre-treated in a flow of 5 % H_2/Ar (400 ^oC, 3h, 20 ^oC min^{-1}).

*Reaction of physical mixture comprising 2.5 % Au 2.5% Pd /TiO_2 and 2.5 % Cu/TiO_2

Table 2 Liquid phase oxidation of methane using heterogeneous Au/Pd/Cu/TiO_2 catalysts with *in-situ* generated H_2O_2

Entry	Catalyst	Product amount (μmol)				Oxygenate Selectivity / % [a]	Methanol Selectivity / %	Oxygenate Productivity [b]	TOF [c]	H_2O_2 Remaining / μmol [d]
		CH_3OH	HCOOH	MeOOH	CO_2					
1	2.5 % Au 2.5 % Pd /TiO_2	1.31	0	0.29	0.32	83	68.2	0.11	0.320	56
2	2.5% % Au 2.5 % Pd 2.5 % Cu/TiO_2	0.45	0	0	0.1	98	81.8	0.068	0.090	18
3	2.5% % Au 2.5 % Pd 1.0 % Cu/TiO_2	0.39	0	0	0.13	75	75.0	0.040	0.078	9
4	2.5 % Au 2.5 % Pd 0.5 % Cu/TiO_2	0.31	0	0	0.20	61	60.8	0.027	0.062	17
5	2.5 % Au 2.5 % Pd 0.25 %Cu/TiO_2	0.25	0	0	0.91	22	21.6	0.020	0.050	14
6	2.5 % Cu/TiO_2	0	0	0	0	0	n/a	0.00	0	0
7	2.5 % Au 2.5 % Pd /TiO_2 and 2.5 %Cu/TiO_2*	0.49	0	0	0.1	98	83.1	0.074	0.098	9

Test conditions: 0.5 h, 50 ^oC, Catalyst: 1.0 x 10^{-5} mol of metal, 1500 rpm, Gases: 0.86 % H_2/ 1.72 % O_2/ 75.86 % CH_4 / 21.55 % N_2, P(Total pressure) = 32 bar

[a] Oxygenate selectivity = (mol of oxygenate/ total mol of products) * 100, [b] Oxygenates productivity = mol $_{oxygenates}$ kg_{cat}^{-1} h^{-1}, [c] Turn over frequency (TOF) = mol $_{oxygenates}$ mol $_{metal}^{-1}$ h^{-1}, [d] Assayed by Ce^{+4} (aq) titration, *Reaction of physical mixture comprising 2.5 wt% Au 2.5 % Pd /TiO_2 and 2.5 % Cu/TiO_2

Table 3 H_2O_2 synthesis and degradation rates for Titania- supported AuPd and AuPdCu catalysts.

Entry	Catalyst	Productivity mol / kg_{cat} / h[a]	Degradation mol / kg_{cat} / h[b]
1	2.5% Au 2.5% Pd / TiO_2	83	215
2	2.5% Au 2.5% Pd 2.5% Cu / TiO_2	11	143
3	2.5% Au 2.5% Pd 1% Cu / TiO_2	10	184

[a] Test conditions: 5% H_2/CO_2 (29 bar) and 25% O_2/CO_2 (11 bar), 8.5 g solvent (2.9 g HPLC water, 5.6 g MeOH) 0.01 g catalyst, 2 ^oC, 1200 rpm, 30 mins).

[b] Test conditions: 5% H_2/CO_2 (29 bar), 8.5 g solvent (5.6 g MeOH, 2.22 g H_2O and 0.68 g 50%H_2O_2), 0.01 g catalyst, 2 ^oC, 1200 rpm, 30 mins.

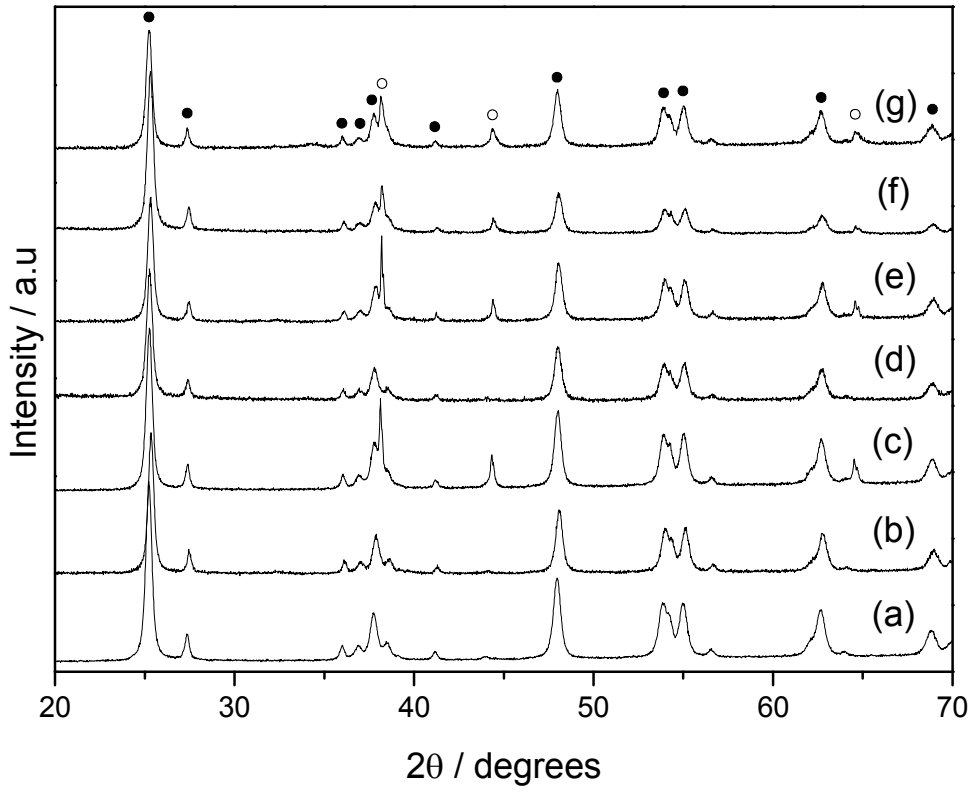

● TiO_2 phase, ○ Au/Au-Pd phase.

Figure 1 XRD diffractograms of TiO_2 deposited with (a) Support only, (b) 2.5 % Cu, (c) 2.5 % Au, (d) 2.5 % Pd, (e) 2.5% Au 2.5% Pd, (f) 2.5 % Au 2.5 % Pd 1.0 % Cu, (g) 2.5 % Au 2.5 % Pd 2.5 % Cu

Table 4 Calculated Au particle properties from XRD

Catalyst	Metal Phase	Unit Cell Volume / Å^3
2.5% Au/TiO_2	Au	67.79
2.5% Au 2.5% Pd/TiO_2	Au	67.84
2.5% Au 2.5% Pd 1.0% Cu/TiO_2	Au	67.73
2.5% Au 2.5% Pd 2.5% Cu/TiO_2	Au	67.51
Reference [a]	Au	67.85

[a] Reference no. ICSD no. 611624

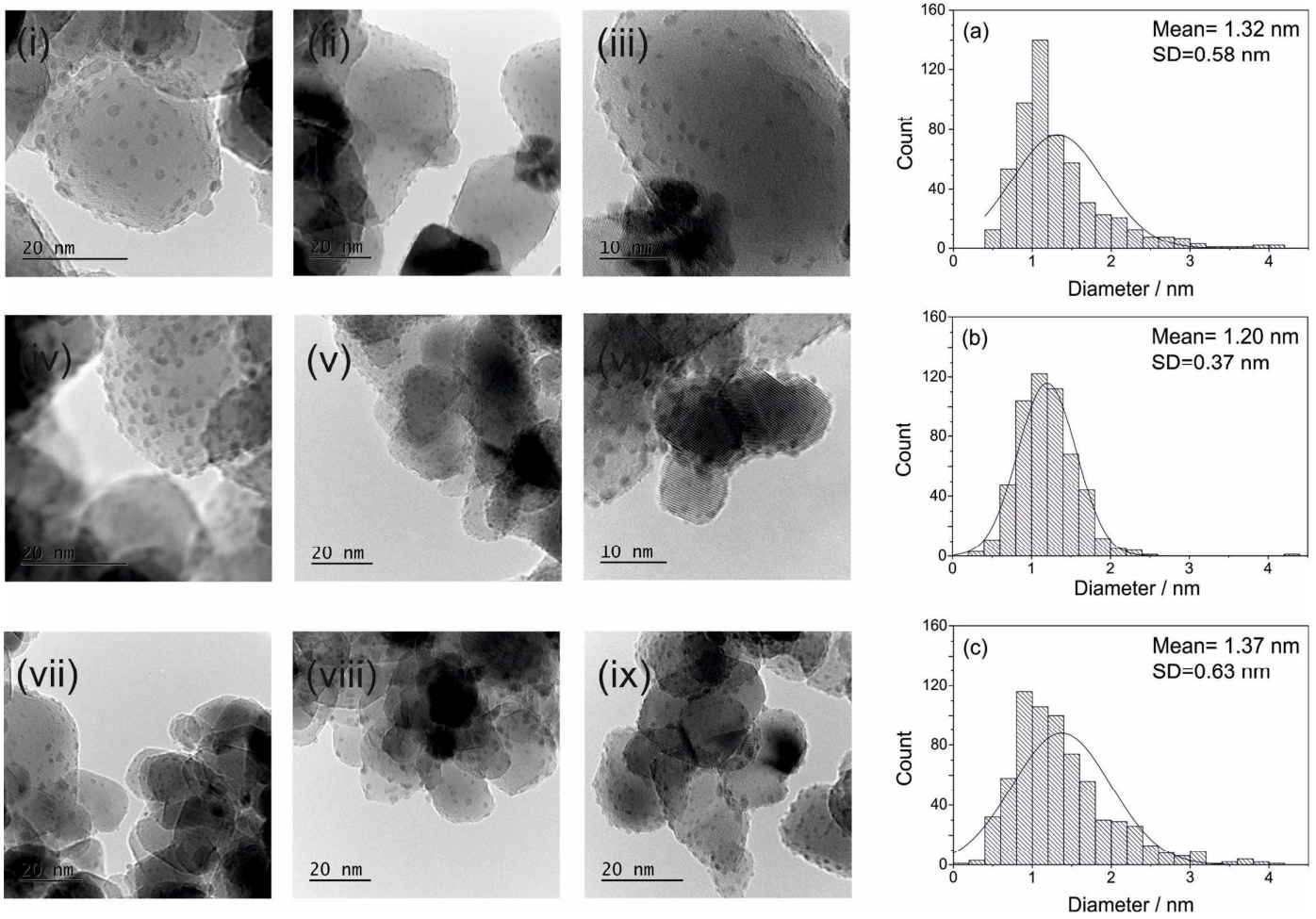

Figure 2 Representative electron micrographs and associated particle size distributions for: (a, i, ii, iii) 2.5% Au 2.5% Pd/TiO_2, (b, iv, v, vi) 2.5 % Au 2.5 % Pd 1% Cu/ TiO_2 and (c, vii, viii, ix) 2.5% Au 2.5% Pd 2.5% Cu/ TiO_2.

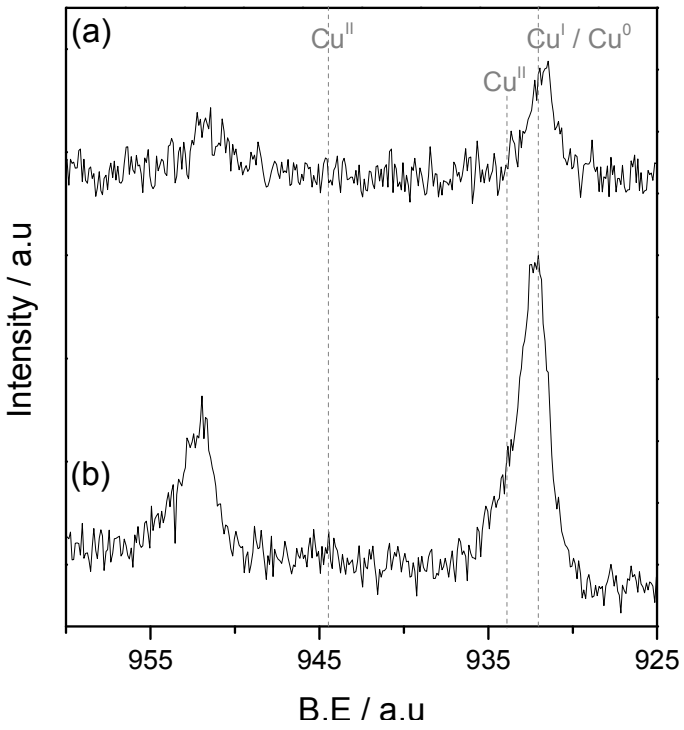

Figure 3 XPS spectra in the Cu (2p) region for 2.5% Au 2.5% Pd 1.0% Cu/ TiO_2 before (a) and after (b) calcination at 400 ^{o}C.

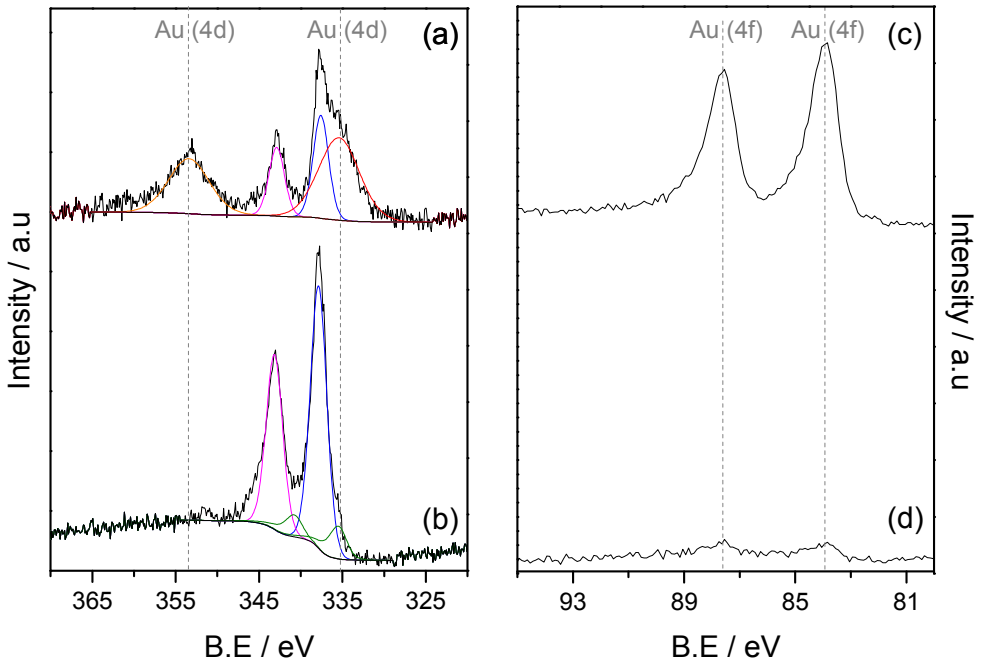

Figure 4 XPS spectra of 2.5% Au 2.5% Pd 1.0% Cu/ TiO_2 before (a, c) and after (b,d) calcination at 400 ^{o}C. Spectra show (a, b) the Au (4d) / Pd (3d) region and (c, d) the Au (4f) region.

Table 5 Surface elemental composition from XPS data for calcined and uncalcined catalysts

Entry	Catalyst	Treatment	Composition / atom %			Atom ratio Pd/Au	Atom ratio Cu/Au	Atom ratio Pd/Cu
			Au/Ti	Pd/Ti	Cu/Ti			
1	2.5% Au 2.5% Pd 2.5% Cu/TiO_2	Uncalcined	0.040	0.022	0.022	0.54	0.54	1.00
2		Calcined	0.003	0.046	0.043	15.17	14.17	1.07
3	2.5% Pd 2.5% Cu/TiO_2	Calcined	-	0.056	0.054	-	-	1.04

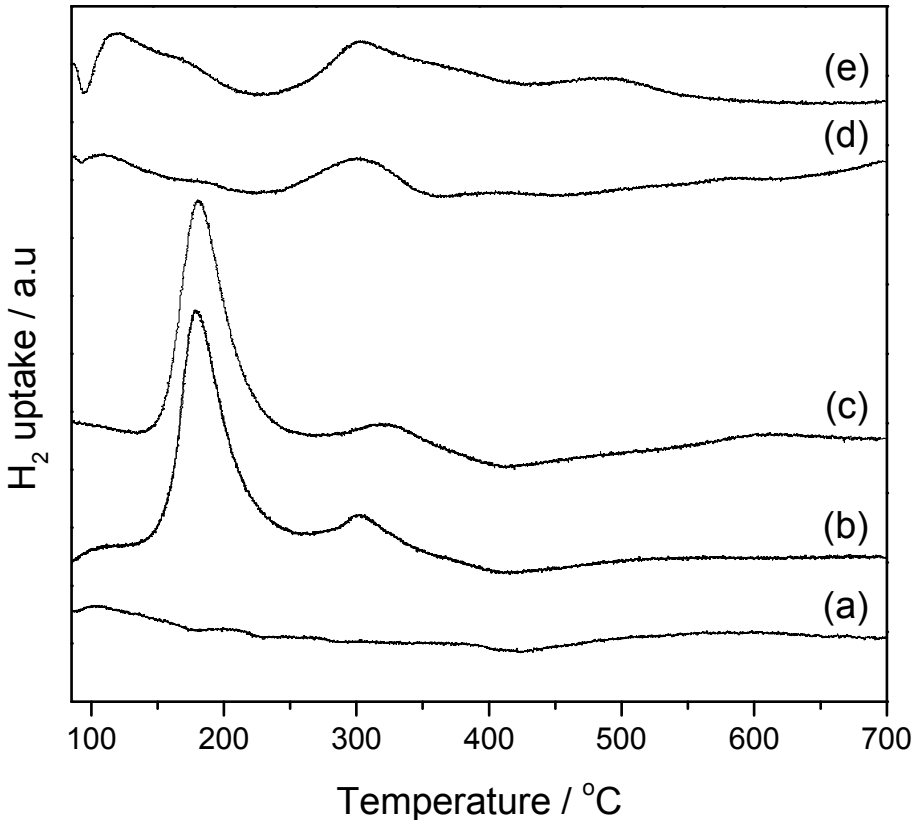

Figure 5 TPR profiles of (a) TiO_2, (b) 2.5 %Cu/TiO_2, (c) 2.5 % Au 2.5 % Cu/ TiO_2, (d) 2.5 % Au 2.5wt% Pd 1.0 % Cu/ TiO_2, (e) 2.5 % Au 2.5 % Pd/ TiO_2.

CH_4

H_2O_2

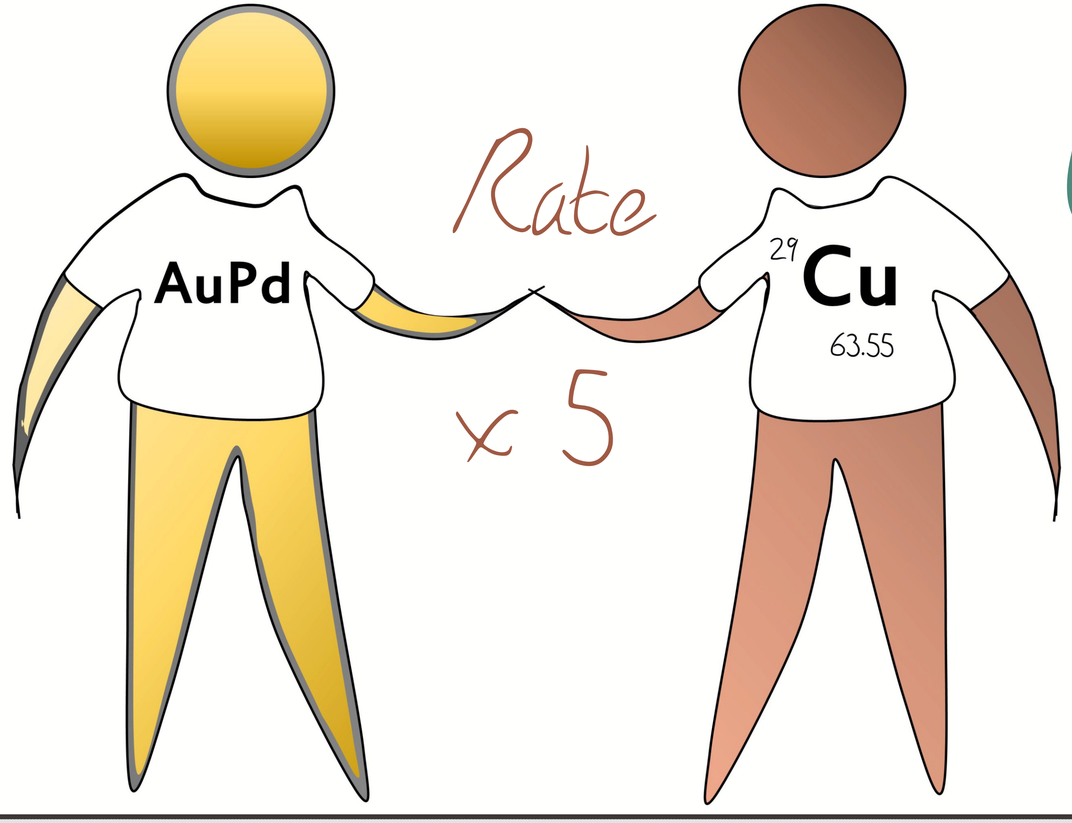

CH_3OH